SECURITY CLASSIFICATION OF THIS PAGE

REPORT DOCUMENTATION PAGE

Form Approved OMB No. 0704-0188

1a. REPORT SECURITY CLASSIFICATION: UNCLASSIFIED	1b. RESTRICTIVE MARKINGS
2a. SECURITY CLASSIFICATION AUTHORITY	3. DISTRIBUTION/AVAILABILITY OF REPORT: Approved for public release; Distribution unlimited.
2b. DECLASSIFICATION/DOWNGRADING SCHEDULE	
4. PERFORMING ORGANIZATION REPORT NUMBER(S): PL-TR-91-2077	5. MONITORING ORGANIZATION REPORT NUMBER(S)
6a. NAME OF PERFORMING ORGANIZATION: Phillips Lab, Geophysics Directorate; 6b. OFFICE SYMBOL (If applicable): OPI	7a. NAME OF MONITORING ORGANIZATION
6c. ADDRESS (City, State, and ZIP Code): Hanscom Air Force Base, Massachusetts 01731	7b. ADDRESS (City, State, and ZIP Code)
8a. NAME OF FUNDING/SPONSORING ORGANIZATION; 8b. OFFICE SYMBOL (If applicable)	9. PROCUREMENT INSTRUMENT IDENTIFICATION NUMBER
8c. ADDRESS (City, State, and ZIP Code)	10. SOURCE OF FUNDING NUMBERS

PROGRAM ELEMENT NO	PROJECT NO.	TASK NO	WORK UNIT ACCESSION NO
61102F	2310	G4	27

DTIC ELECTE MAY 0 6 1991 S D

11. TITLE (Include Security Classification)
$NH(X^3\Sigma^-, v=1\text{-}3)$ Formation and Vibrational Relaxation in Electron-Irradiated $Ar/N_2/H_2$ Mixtures

12. PERSONAL AUTHOR(S)
James A. Dodd, Steven J. Lipson, Dorothy J. Flanagan, William A.M. Blumberg, (see over)

13a. TYPE OF REPORT	13b. TIME COVERED	14. DATE OF REPORT (Year, Month, Day)	15. PAGE COUNT
Reprint	FROM _____ TO _____	1991 April 22	10

16. SUPPLEMENTARY NOTATION
Reprinted from the Journal of Chemical Physics, Vol. 94, p.4301

17. COSATI CODES		
FIELD	GROUP	SUB-GROUP

18. SUBJECT TERMS (Continue on reverse if necessary and identify by block number)
NH, Imidogen, Imine, Vibrational Relaxation, Vibrational Distribution, Chemical Quenching

19. ABSTRACT (Continue on reverse if necessary and identify by block number)

Measurements of the dynamics of $NH(X^3\Sigma^-, v=1\text{-}3)$ created in electron-irradiated N_2/H_2 and $Ar/N_2/H_2$ mixtures, have been performed. Time-resolved Fourier spectroscopy was used to observe $NH(v \rightarrow v\text{-}1)$ vibrational fundamental band emission. Time-dependent populations were then determined by spectral fitting. Subsequent kinetic fitting of these populations using a single-quantum relaxation model and a power-law dependence of k_v on v yielded the following $NH(v=1\text{-}3)$ relaxation rate constants (units of 10^{-14} $cm^3 s^{-1}$): $k_{v=1}(N_2) = 1.2\pm0.5$, $k_{v=2}(N_2) = 3.8\pm1.5$, $k_{v=3}(N_2) = 7.5\pm2.5$; $k_{v=1}(Ar) = 0.2\pm0.1$, $k_{v=2}(Ar) = 0.5\pm0.2$, $k_{v=3}(Ar) = 0.8\pm0.3$; $k_{v=1}(H_2) \leq 50$, $k_{v=2}(H_2) \leq 100$, $k_{v=3}(H_2) \leq 150$. In addition, the N_2/H_2 data provided a measurement of the nascent excited vibrational state distribution resulting from the reaction $N(^2D)+H_2 \rightarrow NH(X,v)+H$. The ratio NH(1):NH(2):NH(3) was found to be 1.0:0.97:0.81 (±0.28 in each value).
(see over for continuation)

20. DISTRIBUTION/AVAILABILITY OF ABSTRACT	21. ABSTRACT SECURITY CLASSIFICATION
☐ UNCLASSIFIED/UNLIMITED ☒ SAME AS RPT. ☐ DTIC USERS	UNCLASSIFIED

22a. NAME OF RESPONSIBLE INDIVIDUAL	22b. TELEPHONE (Include Area Code)	22c. OFFICE SYMBOL
Steven J. Lipson	(617) 377-3626	PL (AFSC)/OPI

DD Form 1473, JUN 86 — Previous editions are obsolete. — SECURITY CLASSIFICATION OF THIS PAGE

UNCLASSIFIED

12. AUTHORS, CONT.

James C. Person (Physical Sciences Inc.), and B. David Green (Physical Sciences Inc.)

19. ABSTRACT, CONT.

Comparison of the observed nascent distribution with that of a statistical model suggests that the ratio NH(0):NH(1) = 0.47. Using this derived distribution, we find the average product level $\langle v \rangle = 1.6$, and the fraction of the available product energy in vibration $\langle f_v \rangle = 0.44$. The present evidence confirms that a single reaction mechanism dominates NH formation, and suggests that the reaction proceeds by direct H atom abstraction rather than the formation of a long-lived H-N-H intermediate.

NH($X^3\Sigma^-$, v=1–3) formation and vibrational relaxation in electron-irradiated $Ar/N_2/H_2$ mixtures

James A. Dodd,[a] Steven J. Lipson, Dorothy J. Flanagan,[b] and William A. M. Blumberg
Geophysics Laboratory (AFSC)/OPI, Hanscom Air Force Base, Massachusetts 01731

James C. Person and Byron David Green
Physical Sciences Inc., 20 New England Business Center, Andover, Massachusetts 01810

(Received 24 October 1990; accepted 14 December 1990)

Measurements of the dynamics of NH($X^3\Sigma^-$, v = 1–3), created in electron-irradiated N_2/H_2 and $Ar/N_2/H_2$ mixtures, have been performed. Time-resolved Fourier spectroscopy was used to observe NH($v \rightarrow v-1$) vibrational fundamental band emission. Time-dependent populations were then determined by spectral fitting. Subsequent kinetic fitting of these populations using a single-quantum relaxation model and a power-law dependence of k_v on v yielded the following NH(v = 1–3) relaxation rate constants (units of 10^{-14} cm^3 s^{-1}): $k_{v=1}(N_2) = 1.2 \pm 0.5$, $k_{v=2}(N_2) = 3.8 \pm 1.5$, $k_{v=3}(N_2) = 7.5 \pm 2.5$; $k_{v=1}(Ar) = 0.2 \pm 0.1$, $k_{v=2}(Ar) = 0.5 \pm 0.2$, $k_{v=3}(Ar) = 0.8 \pm 0.3$; $k_{v=1}(H_2) \leq 50$, $k_{v=2}(H_2) \leq 100$, $k_{v=3}(H_2) \leq 150$. In addition, the N_2/H_2 data provided a measurement of the nascent excited vibrational state distribution resulting from the reaction $N(^2D) + H_2 \rightarrow NH(X,v) + H$. The ratio NH(1):NH(2):NH(3) was found to be 1.0:0.97:0.81 ($\pm$0.28 in each value). Comparison of the observed nascent distribution with that of a statistical model suggests that the ratio NH(0):NH(1) = 0.47. Using this derived distribution, we find the average product level $\langle v \rangle = 1.6$, and the fraction of the available product energy in vibration $\langle f_v \rangle = 0.44$. The present evidence confirms that a single reaction mechanism dominates NH formation, and suggests that the reaction proceeds by direct H atom abstraction rather than the formation of a long-lived H–N–H intermediate.

I. INTRODUCTION

The imidogen radical NH($X^3\Sigma^-$) is a species of fundamental scientific interest. NH is closely analogous to the isoelectronic triplet species CH_2^- and ground state O(^3P), which have received a great deal of attention. Also, because NH has a relatively small number of electrons, its electronic structure and properties are amenable to calculation. However, aspects of the dynamics of NH remain poorly understood. For instance, while studies of excited state [e.g., NH($a^1\Delta$)] quenching by buffer gases have been published,[1,2] the rotational and vibrational dynamics of ground state NH(X,v) have not been reported. NH is known to play an important role in the combustion of nitrogenous materials, such as hydrazine fuels.[3] NH has also been observed in astrophysical objects, including comets and certain types of stars.[4] Thus, knowledge of NH reaction dynamics is needed to characterize NH in numerous chemical and physical processes.

Studies have been performed at the Geophysics Laboratory to understand the dynamics of formation and relaxation of NH(X,v = 1–3) created by the interaction of a 35 kV electron beam with gas mixtures containing N_2, H_2, and Ar. NH(v) fundamental band infrared emission was first observed in electron-irradiated N_2/H_2 mixtures by Green and Caledonia.[5] By selectively quenching pathways involving ionic precursors, they determined that the observed NH(v) was produced by the reaction

$$N(^2D) + H_2 \rightarrow NH(v \leq 3) + H. \quad (1)$$

An N(^2D) precursor is favored over ground state N(^4S), since $N(^4S) + H_2 \rightarrow NH + H$ is endothermic, and also over the higher energy N(^2P) state, for which no adiabatic pathway exists connecting reactants to products.[6] In addition, the exothermicity of reaction (1) permits formation of NH($v \leq 3$), consistent with observation. Piper *et al*.[7] have measured the rate constant for quenching of N(^2D) by H_2 to be 2.3 ± 0.5 (-12) cm^3/s (read as 2.3×10^{-12}). While N(^2D) is probably quenched by H_2 primarily through reaction (1),[7] the branching ratio between reaction (1) and nonreactive quenching has not been measured.

We have performed two series of experiments concerning NH(v) formation and deactivation, each consisting of about 175 runs under variable conditions of pressure and electron beam parameters. The first series involves mixtures of N_2 and H_2 only, while the second involves mixtures of Ar, N_2, and H_2. Rate constants for the relaxation of NH(v = 1–3) by collision with Ar, N_2, and H_2 have been determined (for Ar and N_2) and bounded (for H_2). In addition to relaxation rate constants, the N_2/H_2 mixture data provide information on the relative formation rates for NH(v = 1–3). Given the mechanism for formation of NH(v) in reaction (1), the observed relative formation rates can be equated to the nascent vibrational distribution. To our knowledge, this experiment provides the first measurement for NH(v) relaxation rate constants and for the nascent vibrational distribution resulting from reaction (1).

[a] Currently at Stewart Radiance Laboratory, 139 Great Road, Bedford, MA 01730.
[b] Current address: 32 Duggan Road, Acton, MA 01720.

 0021-9606/91/064301-10$03.00

II. EXPERIMENTAL

The experiments were performed using the room-temperature LABCEDE apparatus, which has been described in previous publications.[8,9] A pulsed 35 kV electron beam excites a mixture of gases in a 5.4 liter, stainless steel vacuum chamber ("target chamber"), connected to a mechanical pump. Computer-produced pulses were transmitted over a fiber optic link to a high-speed transistor controlling the electron beam grid voltage, enabling beam switching times of about 5 μs. For the N_2/H_2 study, the electron beam was pulsed on for either 300 or 600 μs, with 7.5–30 ms between pulses. The instantaneous current observed at the target chamber was 2.3–3.3 mA. For the $Ar/N_2/H_2$ study, smaller doses were used: pulse widths of 300–600 μs, repeated at 20 ms intervals, with currents of 0.6–1.5 mA.

Argon, nitrogen, and hydrogen (all 99.999%) were used without further purification. Calibrated flow controllers and a 0–100 Torr pressure transducer were used to regulate gas flows and partial pressures. Flow rates and pressures were as follows: For the N_2/H_2 study, N_2, 3810 sccm, 4–25 Torr; H_2, 20–100 sccm, 0.05–0.40 Torr. For the $Ar/N_2/H_2$ study, Ar, 0–5000 sccm, 0–18 Torr; N_2, 1000–5000 sccm, 4–21 Torr; H_2, 40–500 sccm, 0.08–1.00 Torr. Fast flow rates and short residence times were used to minimize buildup of beam-created quenchers in the target chamber. For the $Ar/N_2/H_2$ study the gases were passed through a coiled copper tube cooled to -78 °C to eliminate possible H_2O contamination.

For N_2/H_2 mixtures, observed fluorescence both during and following beam excitation is dominated by $NH(v \rightarrow v-1)$ and $N_2(B-A)$ first-positive band emission. The N_2 first-positive band emission does not obscure $NH(v)$ emission. On the other hand, electron irradiation of $Ar/N_2/H_2$ mixtures results in intense Ar* emission during the beam pulse, which does obscure $NH(v)$ fluorescence; 20 μs after termination of the beam pulse, the Ar* fluorescence is fully quenched, and $NH(v)$ emission can be observed without interference.

$NH(v)$ emission was observed at a 90° angle to the electron beam using a slow-scan Michelson interferometer operated with an InSb detector. The $NH(v \rightarrow v-1)$ vibrational fundamental band emission region of 2500–3400 cm^{-1} is near the peak of the spectral response of the detector. Helium–neon laser fringes were used to monitor displacement of the moving mirror in the interferometer. Spectra were obtained with 15–20 cm^{-1} FWHM resolution, corresponding to 1024 He–Ne reference laser fringes. Fluorescence decay information from 50 electron-beam duty cycles was averaged during each fringe in order to improve the S/N.[9] For the N_2/H_2 runs, the sample spacing was limited to a minimum of 25 μs by the PDP 11/40 data-taking computer; for the $Ar/N_2/H_2$ runs, a Masscomp 5300 computer enabled sample spacings as small as 3 μs and better characterization of observed infrared fluorescence decay. The detector output was successively passed through a matched preamplifier (factor of 10 gain) and a PAR 113 preamplifier with 1 Hz low-frequency and 10 kHz high-frequency rolloff settings (factor of 200–1000 gain), and then digitized. After each run, the averaged, time-ordered interferograms were transferred to Apollo DN3000 and DN10000 computers for further analysis.

Blackbody radiation produces significant modulation in the observed interferograms, resulting in a spectral baseline which rises with decreasing frequency at wavenumbers < 2500 cm^{-1}. Thus, to permit the observation of possible features in this region, an interferogram taken long after termination of the *e* beam (i.e., after all molecular emission has been quenched) was subtracted from $NH(v)$ interferograms. Fast Fourier transformation[10] of the resultant interferograms generated real, time-ordered fluorescence spectra. Each double-sided interferogram was zero-filled to 8192 points to give an adequate spectral point density. The wavenumber dependence of the phase of the transform was corrected[11] by subtracting a reference phase. The reference phase was determined by transforming a triangularly apodized center portion of the interferogram, corresponding to 60 He–Ne laser fringes. Finally, spectral fitting was performed, described in detail in the next section.

Calibration of the spectral response of the detection system was accomplished using an Infrared Industries model 408 source to produce 1000 °C blackbody radiation. This radiation was expanded with a CaF_2 telescope to fill the field-of-view of the detector. The response was checked near the end of the study by reflecting the blackbody radiation with a Labsphere model IRT-94-020 factory-calibrated gold-coated diffuse reflector to fill the field-of-view. The two methods gave consistent calibration curves.

III. SPECTRAL FITTING OF NH(v) CHEMILUMINESCENCE

A typical $NH(v)$ emission spectrum corrected for detector spectral response is shown in Fig. 1. Emission from upper-state population in $v = 1$–3 is evident. No fluorescence is observed in the overtone region, which also lies well within the spectral range of the detector. All spectra were fit

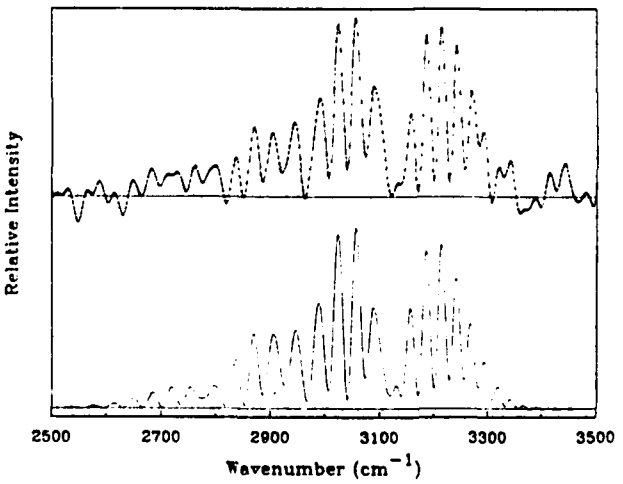

FIG. 1. Typical observed $NH(v)$ vibrational fundamental band emission spectrum, corrected for spectral response. Data points have been connected by straight lines. Emission from $v = 1$–3 is observed. A spectral fit is shown offset beneath the spectrum; zero lines are included for both plots. Pressures used: 21.0 Torr N_2, 0.08 Torr H_2. Electron beam parameters: 35.0 kV, 1.5 mA at the target chamber, 0.6 ms duration, 19.5 ms between pulses. Spectrum was taken 30 μs after beam termination.

in the wave number range 2500–3400 cm^{-1}.

The spectral analysis of NH(v) is complicated by the lack of validated, accurate Einstein coefficients for infrared fundamental band emission. No calculated set is available in the literature. Thus, we have adopted the following approach: For the relative vibrational bandstrengths, A_v coefficients were obtained by computing[12] matrix elements $|\langle v|\mu(r)|v-1\rangle|^2$. The dipole moment function $\mu(r)$ of Goldfield and Kirby[4,13] was used for the calculation. Rotationless wave functions $\langle v|$ were computed in two steps. First, an NH(X) potential energy function was determined through a Rydberg–Klein–Rees inversion[14] of a set of empirical NH(X) rovibrational term values.[15] The wave functions $\langle v|$ were then calculated from the NH(X) potential function using a Numerov–Cooley algorithm to solve the radial Schrödinger equation.[16] This procedure has been described in more detail elsewhere for the IF($B-X$) system.[17] Table I shows the A_v coefficients obtained from this analysis and used in the spectral fitting procedure to derive time-dependent populations from spectra.

For each vibrational band, the rotational manifold was modeled using the following expression for the relative intensity for a given spin-rotational transition,

$$I_{\Delta N\Delta J}(N,J) = \sigma^4 S_{\Delta N\Delta J}(J)\,\frac{\exp[-E(N,J)/kT]}{Q_{\rm rot}(T)}\,F_{v,v-1}(m). \tag{2}$$

Terms in Eq. (2) are defined as follows: N and J are the upper state rotational angular momentum and total angular momentum excluding nuclear spin, respectively; ΔN and ΔJ are the changes in these parameters resulting from emission. NH($X\,^3\Sigma^-$) closely approximates a Hund's case b molecule, for which $\Delta N = \pm 1$, $\Delta J = 0, \pm 1$ transitions are dipole allowed; transitions with $\Delta N = \Delta J$ dominate, especially at larger J. σ is the frequency of the transition in cm^{-1}; S is the Hönl–London or "linestrength" factor appropriate for a case b molecule.[18] The exponential term is the Boltzmann factor which gives the population in the upper rovibrational state. Rotational term values $E(N,J)$ are taken from Boudjaadar *et al.*,[19] and are used as well to calculate the rotational partition function $Q_{\rm rot}$. Rotational equilibrium is assumed at an effective temperature T. It is seen in practice that at the total pressures used in the LABCEDE experiments (i.e., 4–25 Torr, with a mean collision time of 0.1 μs), rotational equilibrium is achieved on a time scale short compared to the time scale of fluorescence decay (1–8 ms).

$F_{v,v-1}(m)$ is the Herman–Wallis factor accounting for the effect of centrifugal distortion on the rotational dependence of the line intensity,[20] where $m = N$ for R branch transitions and $-(N+1)$ for P branch transitions. The values $F_{v,v-1}(m)$ were computed using

$$F_{v,v-1}(m) = 1 + C_{v,v-1}m + D_{v,v-1}m^2, \tag{3}$$

in which the following values of the coefficients $C_{v,v-1}$ and $D_{v,v-1}$, taken from the semi-empirical results of Chackerian *et al.*,[20] have been used: $C_{10} = 0.062\,77$, $C_{21} = 0.055\,11$, $C_{32} = 0.048\,89$, $D_{10} = 0.002\,251$, $D_{21} = 0.001\,871$, $D_{32} = 0.001\,585$. Spectral fits improved significantly when the Herman–Wallis effect was thus taken into account.

In order to model the observed spectra, line intensities resulting from Eq. (2) were convolved with the self-apodized instrument lineshape of the interferometer. When single-line helium lamp radiation is passed through the interferometer, an interferogram is observed which can be approximated by a linear combination of a rectangularly and a triangularly apodized $\cos(x)$ function, where x is the mirror position. The linearity of the Fourier transformation implies that the instrument lineshape function for a single-line source must be a linear combination of a $\mathrm{sinc}(\sigma)$ and a $\mathrm{sinc}^2(\sigma)$ function. The extent to which each function contributes can be determined by fitting either the single-line spectrum or a molecular emission spectrum such as NH(v), provided the lines have well-known positions and are adequately spaced. The lineshape function depends on the total pressure in the target chamber, presumably due to variation in the spatial distribution of the emitting volume with gas density. This effect was taken into account in the spectral fitting that determined time-dependent NH(v) populations.

To determine lineshape parameters for experimental data, several NH(v) spectra were first fit using a nonlinear least-squares algorithm.[21] In these fits the parameters FWHM linewidth Δ, fraction sinc function α, and rotational temperature T were allowed to vary. Best-fit values of T were near room temperature. These parameters were then fixed in computing three basis sets for $v = 1$–3, each basis set consisting of the set of lines $I_{\Delta N\Delta J}(N,J)$ convolved with the instrument lineshape, then multiplied by the factor A_v. Linear least-squares fits to observed spectra using these basis sets gives three multipliers, which are the relative populations. Figure 2 shows the three basis functions used in the least-squares fit to the spectrum in Fig. 1. Repeating the fit at all times sampled both during and following beam pulse excitation of the gas mixture yields population decay curves for $v = 1$–3, which can then serve as input to the kinetic analysis of the system.

Since both angular divergence and off-axis entrance of fluorescence into a Michelson interferometer can result in apparent red shifts, a lineshift parameter δ, proportional to frequency, was also introduced into the nonlinear fits. Fitted values for δ were $<0.1\%$ of the frequency—more typically 0.02%—a small fraction of the spectral resolution, and too small to significantly affect the quality of the fits.

As discussed previously,[8] spectra not corrected for the detection system response show equal noise at all wave-number values; division by the spectral correction function results in a noise level which increases with wave number for this system. Thus, points were statistically weighted as the inverse of the spectral correction function in the linear fits,

TABLE I. Calculated Einstein coefficients $A_{v,v-1}$ for NH($X\,^3\Sigma^-$, v).

v	$A_{v,v-1}$ (s^{-1})
1	51.7
2	92.3
3	144.4

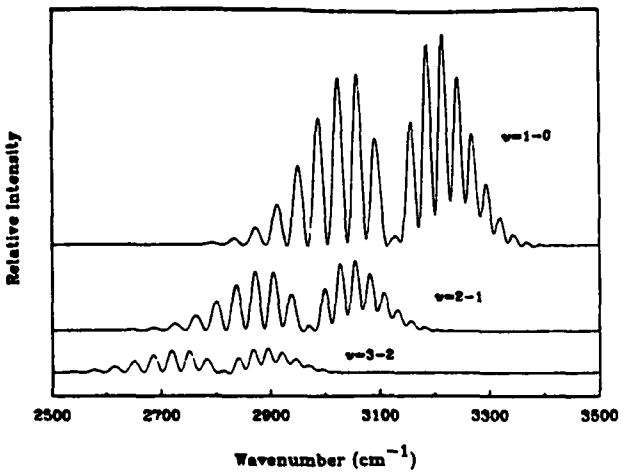

FIG. 2. Basis functions for $v = 1$–3 multiplied by the population factors determined in the best least-squares fit to the spectrum in Fig. 1. Parameters used in basis functions: lineshape parameter $\alpha = 0.24$, FWHM $\Delta = 14.3$ cm^{-1}, rotational temperature $T = 300$ K.

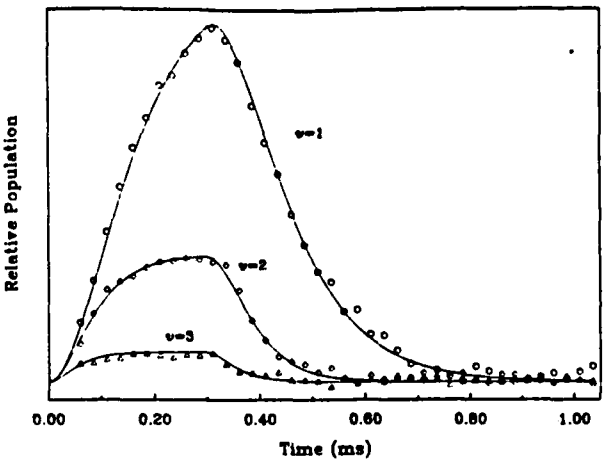

FIG. 3. Run consisting of NH(v = 1–3) time-dependent populations derived from spectral fits to N_2/H_2 data. The e beam turns on at $t = 0$ ms and turns off at $t = 0.30$ ms. While the beam is on the NH(v = 1–3) populations are seen to increase; decays following beam termination are caused mainly by collisional relaxation. Also shown is a kinetic fit (solid curves) to numerous runs of this type, which determines k,α (N_2) and relative creation rates for $v = 1$–3. Pressures used: 15.2 Torr N_2, 0.20 Torr H_2.

placing more importance on data near the red end of the spectrum where the detector is most sensitive. The detection system is about 40% less sensitive at 3400 cm^{-1} than at 2500 cm^{-1}.

The spin-rotational envelope for a given v level is fit well using Eq. (2), judging by the near-unity value of Q arising from the fitting program.[21] (Q is the probability that the value of χ^2 resulting from a spectral fit has occurred as a result of data uncertainty, and not through application of an incorrect model.) Thus we have some confidence in the line-strength factor/Herman–Wallis coefficient approach to the line intensities. Clearly, the accuracy of the fitted populations p_v also depends on the accuracy of the probabilities $A_{v,v'}$ since products $A_{v,v'} \cdot p_v$ result as best-fit values. However, the relaxation rate constants $k_v(M)$ are totally insensitive to the absolute values of the probabilities, and relatively insensitive to probability ratios. Thus, we find that the variation in rate parameters calculated when probability ratios are varied by $\pm 20\%$ is well within the uncertainty arising from other sources. The nascent vibrational distribution determined from the kinetic analysis is somewhat more sensitive to the probability ratios $A_{v,v'}/A_{v,v''}$. The error bars associated with the branching fractions have been increased to take this additional uncertainty into account.

IV. KINETICS METHODS AND RESULTS

The spectral fits produce a family of curves describing population evolution of NH(v = 1–3) over time. Figure 3 shows these populations evolve both during and following the beam pulse. NH(v) populations could be determined at all times from the N_2/H_2 data set. As mentioned above, intense Ar* fluorescence prevents observation of NH(v) during the beam pulse for the $Ar/N_2/H_2$ data set. Owing to this difference, two different approaches were taken in the kinetic analyses of the two data sets; these approaches are explained in detail below.

For the kinetic analyses, we are guided by the results of a similar analysis for the OH(v)/O_2 system.[8] It was shown that severely correlated and uncertain best-fit parameters result when more than one kinetic parameter is introduced for each v level in the fit. Thus, in practice it is not feasible to accurately determine kinetic parameters describing all possible decay channels, including multi-quantum decay and reactive loss. Studies of other systems such as OH(v = 1–3),[8] NO(v = 1–7),[22] and CO(v = 1–16)[9] have shown that a single-quantum mechanism can be used to successfully model vibrational relaxation in diatomic molecules; it is the one we use here.

No exothermic pathways exist for the reaction of NH($v \leq 3$) with the bath gases Ar and N_2. This observation is consistent with the measured upper limit of $3(-19)$ cm^3/s for the rate constant describing reaction between NH and N_2.[23] In the case of H_2, however, the reaction

$$\mathrm{NH} + \mathrm{H_2} \rightarrow \mathrm{NH_2} + \mathrm{H},$$
$$\Delta H^0 = 0.61 \pm 0.06 \text{ eV} \quad \text{(Refs. 24,25)} \qquad (4)$$

becomes exothermic for NH($v \geq 2$). Thus, while reaction (4) does not occur for vibrational ground state NH [$k \lesssim 1(-17)$ cm^3/s (Ref. 26)], it could play a significant role for higher v levels.

The electron beam bombardment of N_2 and H_2 also gives rise to species which are not directly monitored in our experiment, notably NH(v = 0) and N and H atoms. All of these species react rapidly with NH:

$$\mathrm{NH} + \mathrm{NH} \rightarrow \text{products}, \quad 8.5(-11)\text{cm}^3/\text{s(Ref. 27)}, \qquad (5)$$

$$\mathrm{NH} + \mathrm{N} \rightarrow \mathrm{N_2} + \mathrm{H}, \quad 1.8(-11)\text{cm}^3/\text{s(Ref. 3)}, \quad 5.0(-11)\text{cm}^3/\text{s(Ref. 28)}, \qquad (6)$$

$$\mathrm{NH} + \mathrm{H} \rightarrow \mathrm{H_2} + \mathrm{N}, \quad 3.0(-12)\text{cm}^3/\text{s(Ref.3)}, \quad 1.66(-10)\text{cm}^3/\text{s(Ref. 28)}, \qquad (7)$$

$$\mathrm{NH}(v) + \mathrm{M} \rightarrow \mathrm{NH}(v-1) + \mathrm{M}, \quad \mathrm{M} = \mathrm{H,N}. \qquad (8)$$

Spencer and Glass[29] measured the rate constant for deactivation of OH($v = 1,2$) by H and found it to be gas kinetic;

the relaxation of NH(v) by H atoms may also be fast. Previous work on the NH system[5] has shown that ionic pathways lead predominantly to the production of H atoms. Also, as demonstrated by our modeling studies (see below), the populations of the beam-created species are complicated functions of pulse width, beam current, duty cycle, and gas pressure. In this work we have used conditions which should minimize build-up of these quenchers in the target chamber.

Ideally, the data allow relaxation rates to be determined independently for all three observed v levels. Population in NH($v=3$), however, was present in relatively small quantity compared with NH($v=1,2$), with poorer S/N (Fig. 3). Because of the small signal for $v=3$, relaxation rates for $v=3$ could not be determined from the data with acceptable precision. On the other hand, the effect of feed from $v=3$ into lower v levels is significant and must be taken into account in the empirical model. In order to fit the data with fewer parameters, a power law dependence $k_v(M) = v^{\alpha} k_{v=1}(M)$ was assumed for each relaxer gas M. Such a dependence has been found to hold for numerous systems,[30] and represents a minimal constraint on the empirical model. The adjustable parameters $k_{v=1}$ and α are largely determined by the $v=1,2$ levels, which have greater S/N. Rate constants for $v=1,2$ are thus determined with greater precision than those for $v=3$.

Data were fit to both NH growth and decay parameters using the formulae:

$$\frac{d[\mathrm{NH}(1)]}{dt} = \gamma_{v=1} P(t) - R_{v=1}[\mathrm{NH}(1)] + R_{v=2}[\mathrm{NH}(2)], \tag{9}$$

$$\frac{d[\mathrm{NH}(2)]}{dt} = \gamma_{v=2} P(t) - R_{v=2}[\mathrm{NH}(2)] + R_{v=3}[\mathrm{NH}(3)], \tag{10}$$

$$\frac{d[\mathrm{NH}(3)]}{dt} = \gamma_{v=3} P(t) - R_{v=3}[\mathrm{NH}(3)]. \tag{11}$$

The first term in Eqs. (9)–(11) describes the effects of chemical feed from the $N(^2D) + H_2$ reaction; $\gamma_{v=1\text{-}3}$ are coefficients giving the relative feed rate into NH($v=1$–3), and $P(t)$ is a function describing the time dependence of the precursor concentration; it is discussed in more detail below. Because the function $P(t)$ includes a multiplicative factor (see below), the four parameters $\gamma_{v=1\text{-}3}$ and $P(t)$ include a redundancy; thus, in the fits $\gamma_{v=1}$ is set to unity and $\gamma_{v=2,3}$ are solved as fractions of the $v=1$ feed rate. Relative creation rates for NO($v=1$–7) have been analyzed in a similar fashion.[31]

The second and third terms represent decay from and feed into, respectively, a given level v. Single-quantum decay rate parameters R_v are defined by

$$R_v = \{\Sigma v^{\alpha(M)} k_{v=1}(M)[M]\} + R_{v,0}, \tag{12}$$

where the sum is over all of the bath gases (Ar, N_2, H_2) present in the reaction chamber. Here, $R_{v,0}$ is residual NH($v=1$–3) loss, due largely to quenching by beam-created species, which we assume to be a constant over the gas pressures used in these experiments. This assumption, while only an approximation, is supported by the results of both the empirical fits and the kinetic modeling (see below). Single-quantum radiative rates A_{v-v-1} contribute only to the quantities $R_{v,0}$, and double-quantum radiative rates A_{v-v-2} are negligible compared to other terms.

The time dependence of the $N(^2D)$ concentration is given by $P(t)$, mentioned above. Assuming that the rate of formation of $N(^2D)$ is constant during the e beam and zero after beam turn-off, $P(t)$ is given by

$$P(t) = C[1 - \exp(-R_p t)] \tag{13}$$

while the e beam is on, and

$$P(t) = C \exp[-R_p (t - t_b)] \tag{14}$$

while the e beam is off, where the beam turns on at $t=0$ and turns off at $t=t_b$, and C is a constant. The precursor decay rate R_p is given by

$$R_p = \{\Sigma k_p(M)[M]\} + R_{p,0}, \tag{15}$$

where the sum is over the bath gases Ar, N_2, and H_2, and $R_{p,0}$ describes residual $N(^2D)$ loss which we assume to be a constant with respect to gas pressure. The following values for $k_p(M)$ were used (units of cm^3/s): $k_p(H_2) = 2.3(-12)$;[7] $k_p(N_2) = 1.5(-14)$;[32] $k_p(Ar) = 1.0(-16)$.[33]

The rates R_v and the precursor population $P(t)$ are functions of gas partial pressures, and thus depend on the particular data run being examined. However, the rate constants, $k_{v=1}(M)$ and $\alpha(M)$ (M = Ar, N_2, H_2), the creation rate multipliers $\gamma_{v=1\text{-}3}$, and the residual quenching rates $R_{v,0}$ and $R_{p,0}$ are independent of individual run conditions. Therefore, a "global" fitting technique was used in which the time-dependent populations were fit simultaneously for these parameters. In addition, an adjustable gain parameter C is required for each run. Such a fit was necessitated by our use of $k_{v=1}$ and α as decay rate parameters, since a fit to an individual run cannot determine these two parameters. For a given run the coupled linear differential equations were solved numerically by estimating initial values for the rate parameters, then integrating the equations from the time of e-beam onset until the time of the last data point to produce model curves for $v=1$–3. A nonlinear least-squares fitting routine then iteratively adjusted the parameters to produce the best least-squares fit to the experimental data. The present approach takes the place of the two-step analysis used in our previous study of OH(v) relaxation by O_2,[8] in which data were first fit on a run-by-run basis, and then rate constants determined as the slope of the resultant rates plotted against O_2 partial pressure.

Because the N_2/H_2 and $Ar/N_2/H_2$ data sets were taken under different conditions, the two data sets were fit individually to appropriate subsets of the global parameters described above. Excellent fits resulted when this procedure was followed. The two fits are described below.

The N_2/H_2 data set was first fit using ten global parameters [$k_{v=1}(N_2)$, $\alpha(N_2)$, $k_{v=1}(H_2)$, $\alpha(H_2)$, $\gamma_{v=2,3}$, $R_{v=1\text{-}3,0}$, and $R_{p,0}$]. Because the resulting values of the H_2 kinetic parameters k_v were not different from zero within systematic error, the $k_v(H_2)$ were set equal to zero and the fit repeated. A total of 16680 data points (139 runs, each consisting of 40 population values for each of three vibrational levels at 25 μs intervals) were fit using the re-

maining eight global parameters. A good fit resulted from this model, as evidenced in the 4.3% rms deviation of the fit relative to the largest data point in a given run, which is within the estimated 5% uncertainty in the average data point. For N_2, $k_{v=1} = 1.5(-14)$ cm^3/s and $\alpha = 1.4$ were determined from the fit to the N_2/H_2 data set. The normalized relative formation rates of $NH(v = 1$–$3)$ were found to be 0.36, 0.35, and 0.29, respectively. Best-fit relative formation rates can be equated, in turn, to the nascent vibrational distribution in $NH(v = 1$–$3)$ resulting from $N(^2D) + H_2$. These measured branching fractions are given in the first column of Table II. Figure 3 shows the results of this fit applied to a particular run.

In the second data set, where $Ar/N_2/H_2$ mixtures were used, data were taken after termination of the e beam, and therefore the $NH(v)$ relative creation rates were not used as adjustable parameters. In the absence of literature values for the creation rates, the above rates were used as fixed parameters in the fit. Best-fit values for k,α (Ar,N_2) were found to vary by less than 5% upon 50% variation of the relative creation rates. The $N(^2D)$ decay parameter $R_{p,0}$ could not be determined and was set equal to 5×10^3 s^{-1}, the value obtained from the fit to the N_2/H_2 data. The fit to the $Ar/N_2/H_2$ data also gave poorly determined H_2 kinetic parameters; thus, $k_v(H_2)$ were set equal to zero and the fit repeated. A total of 73308 data points (222 runs, consisting of an average of 110 populations for each of three vibrational levels at 10 μs intervals) were fit using seven global parameters $[k_{v=1}(Ar), \alpha(Ar), k_{v=1}(N_2), \alpha(N_2), R_{v=1\text{-}3,0}]$. The fit resulted in an rms deviation of 3.9%, similar to the rms deviation resulting from the analysis of the N_2/H_2 data. Values of $k_{v=1}(Ar) = 2(-15)$ cm^3/s, $\alpha(Ar) = 1.2$, and $k_{v=1}(N_2) = 1.0(-14)$ cm^3/s, $\alpha(N_2) = 1.9$ were determined from the fit to the $Ar/N_2/H_2$ data set. Figure 4 shows the fit superimposed on data points for a particular run.

Final values for $k_{v=1\text{-}3}(N_2)$ were chosen to be the average of the results from the N_2/H_2 and $Ar/N_2/H_2$ studies, since the two data sets were composed of a similar number of runs, and because the fits were of comparable quality. While the values of the $k_v(N_2)$ resulting from the two fits differ by more than their combined statistical uncertainties, the differences are within the estimated systematic error in the experiment. Neither data set produced values for H_2 kinetic parameters. Instead, upper limits for $k_v(H_2)$ were set at the maximum values which produced acceptable fits. Using this method, $k_{v=1\text{-}3}(H_2) \leq 0.5$, 1.0, and $1.5(-12)$ cm^3/s, respectively, where α has been assumed to be 1.0. All of the relaxation kinetics results are collected in Table III.

Values of $R_{v,0} = 500$–5000 s^{-1} were obtained in the fits to the N_2/H_2 and $Ar/N_2/H_2$ data sets. These values are significantly larger than can be accounted for by either radiative loss or diffusion out of the field-of-view (10 s^{-1} at the lowest pressures used). Instead, these values probably reflect quenching by beam-created species. $NH(v)$ is quenched to some degree by itself and by H and N [Eqs. (5)–(8)]. The $N(^2D)$ residual decay parameter $R_{p,0} = 5000$ s^{-1} determined in the fit to the N_2/H_2 data set is also consistent with efficient quenching of $N(^2D)$ by beam-created species, which could include electrons, ions, and NH.

To investigate the role of beam-created quenchers, a number of runs were taken under various conditions of e-beam pulse width (250–2750 μs) and duty cycle period (4–30 ms), with constant N_2 and H_2 partial pressures. The $NH(v > 0)$ relaxation rate increases linearly with increased pulse width, apart from an offset due to N_2 and H_2 quenching. This result suggests a proportionality relationship between pulse width and the steady-state concentration of beam-created quenchers. The slope implies beam-induced quenching qualitatively consistent with the residual $NH(v)$ loss rates determined in the empirical fits. Assuming a gas-kinetic quenching rate constant of 10^{-10} cm^3/s, a residual loss rate of 1000 s^{-1} implies a steady-state quencher concentration of 10^{13} cm^{-3}, in qualitative accord with expectation. Larger, but still reasonable, quencher concentrations are calculated if one assumes smaller quenching rate constants. The above study determined that the conditions which minimize beam-created quencher activity are pulse width ≤ 600 μs and duty cycle period ≥ 7.5 ms. Within this regime, the empirical model provides a satisfactory description of $NH(v)$ decay due to residual quenching. All data used to determine rate constants were collected under these constraints.

V. MODELING OF REACTION CHEMISTRY

In order to test hypotheses concerning formation mechanisms and reactivity of beam-created species, we have modeled the chemistry of irradiated N_2/H_2 mixtures using a detailed chemical model. The calculations use subroutines from the CHEMKIN chemical kinetics software package,[34] together with estimates of the initial yields of the different reactive species, both neutral and ionic, created by the interaction of the electron beam with the gas mixture. The initial yields were estimated using the Electron Energy Loss Code[35] to determine the effects of the deposited energy. The

TABLE II. Nascent product distribution for $N(^2D) + H_2 \rightarrow NH(X\,^3\Sigma^-, v \leq 3) + H$.

v	Branching fraction: Measured	Prior[a]	Measured + Surprisal[b]
0	...	0.53	0.15
1	0.36 ± 0.10	0.30	0.31 ± 0.09
2	0.35 ± 0.10	0.14	0.30 ± 0.09
3	0.29 ± 0.10	0.03	0.24 ± 0.09

[a] Equation (18).
[b] Branching fraction for $v = 0$ determined from Fig. 6(b).

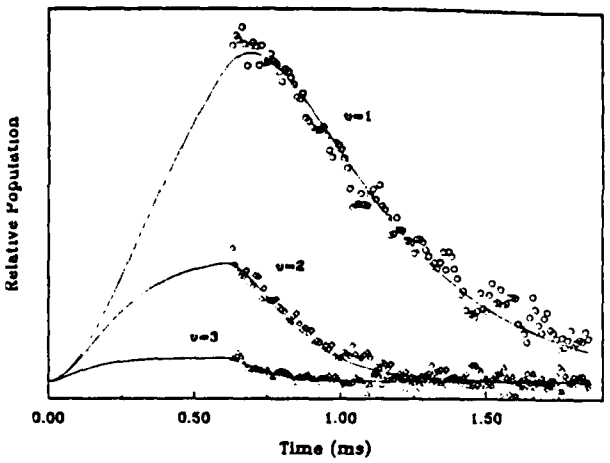

FIG. 4. Run consisting of NH(v = 1–3) time-dependent populations obtained from $Ar/N_2/H_2$ data. The *e*-beam turns on at $t = 0$ ms and turns off at $t = 0.60$ ms. Also shown is a kinetic fit (solid curves) to numerous runs of this type, which determines $k_i\alpha$ (Ar,N_2). Pressures used: 14.3 Torr Ar, 2.9 Torr N_2, 0.08 Torr H_2.

interaction volume was estimated from the relation for the cone angle[16] in pure N_2, while providing for the small effect of added H_2 using scaling based on the ionization cross section. Model calculations typically included 100 reactions.[17]

The kinetic model allows species to evolve in time over multiple duty cycles assuming specified parameters, e.g., gas partial pressures, duty cycle period, and *e*-beam pulse width and current. The most important beam-created species are H atoms and N atoms, both of which reach steady-state concentrations over several *e*-beam duty cycles. The maximum concentrations of the H atoms are 2–10 times the maximum N atom concentrations. For example, in a mixture of 7.5 Torr N_2 and 0.05 Torr H_2, with a 300 μs pulse width, one determines $[H] = 4(13)\ cm^{-3}$, $[N] = 2(13)\ cm^{-3}$, and $[NH] = 3(10)\ cm^{-3}$. These concentrations, when multiplied by the rate constants for reactions (5)–(7), give 480–7640 s^{-1} for the contribution of H, N, and NH to NH(v) quenching, depending on the choice of the rate constants. NH(v) quenching by NH is negligible compared to quenching by H and N atoms. The 480 s^{-1} value is a lower limit, since we have neglected any contribution from reaction (8). Moreover, the lower value for the rate constant for reaction (7) includes the effects of an activation energy of 1000 K, a barrier that may decrease upon vibrational excitation of the NH reactant. Thus, estimated rates for the quenching of NH(v) by H and N are consistent with fitted values $R_{v,0}$.

The kinetic model generates both relaxation rate constants and ratios of NH(v) creation rates. Figure 5 shows values for NH($v = 1$–3) time-dependent populations calculated by the kinetic model, compared with experiment. [Absolute NH(v) concentrations, determined from the model, are consistent with expectation.] The model predicts that among the potential sources for NH(v), N(^2D) plays a much more significant role than other potential sources, such as ionic species and metastable $N_2(A^3\Sigma_u^+)$. With reasonable choices for the kinetic and initial yield parameters, the kinetic model predicts N_2 and H_2 relaxation rate constants and a nascent distribution of NH(v) that are within the limits quoted in Tables II and III. These observations provide further evidence that the observed NH(v) result from $N(^2D) + H_2$.

It is important to draw a distinction between the methodology of the kinetic model and that of the empirical fitting process. The empirical fit does not include a detailed set of reactions, and thus does not address the possible role of beam-created quenchers, other than yielding effective values of $R_{v,0}$ and $R_{p,0}$. The kinetic model, on the other hand, includes numerous reaction pathways. While a number of these reactions have poorly determined rate constants, variation of these rate constants within reasonable limits does not strongly affect predictions made for rates of NH(v) formation and decay. As a result, the model remains in qualitative agreement with the data for a wide range of chosen input parameters. Model predictions did depend, however, on the inclusion of pathways describing quenching of NH(v) by beam-created species, especially H atoms. Thus, the model gives insight into the role of the beam-created N and H atoms on the population of NH($v > 0$). It also provides a

TABLE III. Rate constants for NH($X^3\Sigma^-$, v) + M → NH($v-1$) + M.

v	Rate constant (10^{-14} cm^3 s^{-1}) N_2	Ar	H_2[a]
1	1.2 ± 0.5	0.2 ± 0.1	< 50.
2	3.8 ± 1.5	0.5 ± 0.2	<100.
3	7.5 ± 2.5	0.8 ± 0.3	<150.

[a] May include reactive quenching via reaction (4) for NH($v = 2,3$).

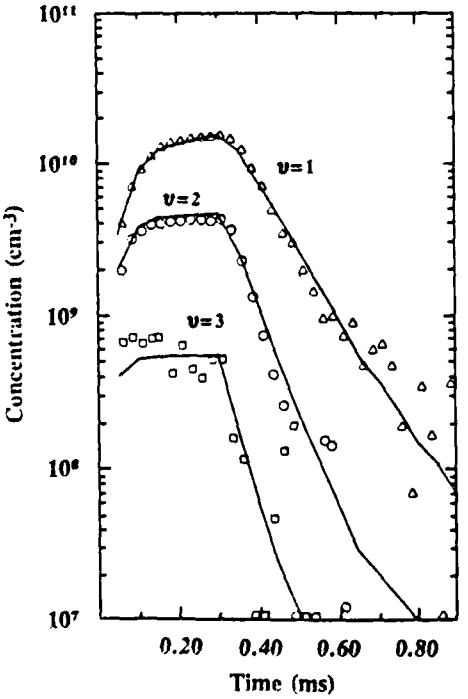

FIG. 5. Semilog plot showing kinetic model for NH(v = 1–3) time evolution superimposed on (normalized) data. The *e* beam turns on at $t = 0$ ms and turns off at $t = 0.30$ ms. Absolute concentrations for NH(v) were determined from the model and not from experiment, which provided only relative populations.

valuable check on possible problems in the empirical fitting process, which, if present, would give rise to poorer agreement.

VI. STATISTICAL ANALYSIS OF PRODUCT VIBRATIONAL DISTRIBUTION

Because we detect product NH(v) in emission, we cannot observe formation of NH($v=0$). However, the nascent yield for NH($v=0$) can be inferred by comparing our results for NH($v=1$–3) with a distribution obtained by assuming a statistical partitioning of the total energy available to the NH(v) product. The statistical model assumes that all product quantum states are equally probable, given the sole constraint of conservation of total energy. This surprisal analysis method has been discussed in numerous reports.[38]

To make a prediction for the relative amount of NH($v=0$), the surprisal $S(f_v)$ is plotted as a function of the reduced energy $f_v = E_v/\langle E_T\rangle$, where E_v is the energy of vibrational state NH(v) relative to NH($v=0$), and $\langle E_T\rangle$ is the average total energy available to the NH(v) product. Thus, f_v is the fraction of the available product energy present in vibration. E_v was calculated for $v=0$–3 using the band origins determined in the spectroscopic study by Boudjaadar *et al.*[19] $\langle E_T\rangle$ is estimated as

$$\langle E_T\rangle = \Delta E^0 + E_a + \tfrac{3}{2}kT + kT, \tag{16}$$

where ΔE^0 and E_a are the reaction energy and activation energy, respectively. The sum $E_a + (3/2)kT$ is the average reactive collision energy, and the last term is the average rotational energy.[39] $\langle E_T\rangle$ is uncertain to $\pm kT$.

To determine ΔE^0, we use the energy cycle

$$\begin{aligned} &N(^2D) + H_2 \rightarrow N(^4S) + H_2 \rightarrow N(^4S) + 2H \\ &\quad \rightarrow NH(^3\Sigma^-) + H, \end{aligned} \tag{17}$$

$$\begin{aligned} \Delta E^0(\text{eV}) &= -2.3846(1) + 4.4781(2) - 3.37(3) \\ &= -1.28(3)\ \text{eV}, \end{aligned}$$

with standard values for $D_0(H_2)$[15] and $E(N(^4S) \rightarrow N(^2D))$.[40] and the recently calculated value for $D_0(NH(^3\Sigma))$.[41] The activation energy E_a in Eq. (16) is taken to be 1 kcal/mole, on the basis of measured activation energies for hydrogen atom transfer reactions with similar ΔH^0.[42] Thus $\langle E_T\rangle = 1.39 \pm 0.04$ eV is the average total energy available to the nascent NH(v) product from $N(^2D) + H_2$.

To perform a surprisal analysis, a "prior" function $P^0(f_v)$ must be defined which describes the prior expectation for the NH(v) product distribution assuming statistical distribution of the available energy. It can be shown[38] that for a three-body reaction such as $N(^2D) + H_2$ the prior function can be approximated by

$$P^0(f_v) = (1-f_v)^{3/2}/\sum_v (1-f_v)^{3/2}, \tag{18}$$

where the sum in the denominator is over all populated product v states, i.e., $v=0$–3. Similar functional dependencies result even when constraints arising from the conservation of angular momentum are taken into account.[38] The prior values calculated using Eq. (18) are plotted along with the measured values for $v=1$–3 in Fig. 6(a).

Figure 6(b) shows a plot of the surprisal function

$$S(f_v) = -\ln[P(f_v)/P^0(f_v)], \tag{19}$$

vs. f_v, where $P(f_v)$ is the observed vibrational distribution. The relationship is seen to be linear, consistent with a single reaction mechanism giving rise to observed NH(v). The surprisal plot yields NH(0):NH(1) = 0.47, suggesting that NH($v>0$) levels are populated more quickly than the ground vibrational state. The middle column of Table II shows the prior distribution of nascent NH(v), while the right-hand column gives the distribution inferred from measurement plus the surprisal analysis.

The negative slope (-3.9) in Fig. 6(b) is indicative of a product vibrational distribution which is more excited than that predicted by the statistical model, i.e., the measured average product level $\langle v\rangle_{meas}$ is larger than the prior prediction $\langle v\rangle_{prior}$. Here, $\langle v\rangle$ is determined from

$$\langle v\rangle = \sum_{v=0}^{3} v\chi_v, \tag{20}$$

where χ_v is the normalized branching fraction. With the data in Table II, Eq. (20) can be used to calculate $\langle v\rangle_{meas} = 1.6$ and $\langle v\rangle_{prior} = 0.7$. In addition, the fraction of the average total product energy in the NH(v) vibration is given by

$$\langle f_v\rangle = \frac{\langle E_v\rangle}{\langle E_T\rangle} = \frac{1}{\langle E_T\rangle}\sum_{v=0}^{3} E_v\chi_v. \tag{21}$$

where $\langle E_v\rangle$ is the average vibrational energy. With Eq. (21) and Table II, one determines $\langle f_v\rangle = 0.44$, substantially larger than the prior value $\langle E_v\rangle_{prior} = 0.18$.

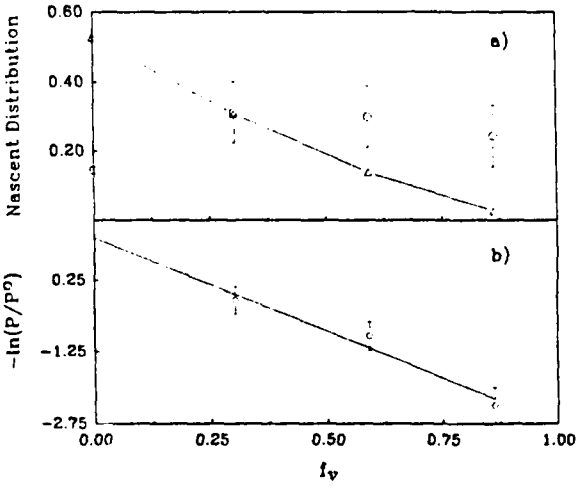

FIG. 6. (a) Calculated and observed nascent vibrational distribution as a function of the reduced energy parameter f_v, the fraction of the available product energy in the NH vibration. Circles are data for $v=1$–3 and triangles are calculated prior values for $v=0-3$ from Eq. (18). The circle at $f_v=0$ is the prediction for $v=0$ made by the surprisal analysis. (b) Surprisal function $-\ln(P/P^0)$ plotted against f_v. The linear relationship is consistent with a single operative mechanism for NH(v) production; the negative slope reflects a product distribution which is more highly excited than the prior expectation. The y intercept gives rise to the prediction for $v=0$ shown in Fig. 6(a).

II. DISCUSSION

Much attention in the field of vibrational energy transfer has focused on the relationship between the single-quantum relaxation rate constant $k_{v\to v-1}$ and v. Qualitatively different behavior has been observed for the vibrational relaxation of diatomic and polyatomic molecules. In general, diatomics relax according to $k_v = v^{\alpha}k_{v=1}$, where $\alpha > 1$, while polyatomics relax according to $k_v = v\,k_{v=1}$.[30] This behavior has been seen for relaxation of the open shell species NO(v = 1–7),[22] where a $v^{1.5}$ dependence was observed, as well as for relaxation of such closed-shell species as HF and CO.[30] For relaxation of NH(v = 1–3) by N_2 and Ar we determine α values of 1.7 ± 0.3 and 1.2 ± 0.3, respectively, indicating behavior intermediate between linear and quadratic dependence on v. Measurements of $k_{v>3}$ will require a different source for NH(v).

Relaxation of NH(v = 1–3) by both N_2 and Ar is extremely inefficient; on average, about 10^4 collisions are required for relaxation by N_2, and 5×10^4 collisions for relaxation by Ar. An efficient V-V transfer mechanism is not available for relaxing NH(v = 1–3) by collision with either N_2 or Ar [$\nu(N_2) = 2330\ cm^{-1}$, ν(NH(v = 1–3)) = 3570–3230 cm^{-1}]. Thus, a V-R and/or V-T mechanism is reflected in the very low observed efficiencies, especially in the case of Ar.

The nascent distribution parameter $\langle f_v \rangle$ can be compared with those arising from the reactions of F atoms with hydrides RH, for which there are abundant data. In general, reactions F + HR → FH + R channel a percentage of the available energy into the product (HF) vibration which is comparable to that of $N(^2D) + H_2$. For instance, the reactions F + HR with group VI hydrides HR = H_2O, CH_3OH, and H_2S yield values $\langle f_v \rangle$ of 0.41, 0.44, and 0.45, respectively.[42] In addition, values $\langle f_v \rangle$ do not seem to depend strongly on the nature of R; it has been shown that for reactions of this type (A + HB → AH + B, with A and B both much heavier than H), a relatively small percentage of the available product energy is channeled into the vibrational energy of the R fragment.

The reaction $N(^2D) + H_2$ can also be compared with reaction (22), which involves an analogous reaction of $N(^2D)$ with a homonuclear diatomic molecule:

$$N(^2D) + O_2 \to NO(v \leq 18) + O(^3P), \quad \Delta E^0 = -3.76\ eV, \tag{22a}$$

$$\to NO(v \leq 8) + O(^1D), \quad \Delta E^0 = -1.79\ eV, \tag{22b}$$

Reaction (22) is complicated by competing product channels giving the ground and first excited states of O, respectively. A recent analysis,[43] however, suggests that reaction (22b) is the more important channel for NO(v) formation. Observed peaking toward high v levels in the product implies a direct abstraction mechanism with a repulsive approach configuration and a short-lived collision complex. The reaction of higher energy $N(^2P)$ with O_2, on the other hand, may occur via a long-lived complex with complete randomization of the reaction energy.[43] In this case large values of J in initially formed product states NO(v,J) are consistent with an attractive approach configuration.

Further comparisons with $N(^2D) + H_2$ can be made by considering reactions (23)–(25), all of which nominally involve hydrogen atom transfer between a second-row atom and H_2:

$$N(^2D) + H_2 \to NH(v \leq 3) + H, \quad \Delta E^0 = -1.28\ eV, \tag{23}$$

$$O(^1D) + H_2 \to OH(v \leq 4) + H, \quad \Delta E^0 = -1.88\ eV, \tag{24}$$

$$F(^2P) + H_2 \to FH(v \leq 3) + H, \quad \Delta E^0 = -1.38\ eV. \tag{25}$$

$F + H_2 \to FH + H$ is one of the most closely studied atom transfer processes. The reaction produces a vibrational distribution which is strongly peaked at $v = 2$.[44] Most of the available product energy is channeled into FH vibration: $\langle f_v \rangle = 0.67$.[44] These observations, along with trajectory studies, suggest that $F + H_2$ proceeds as a direct atom abstraction.[45] Reactions F + HR → FH + R mentioned above probably involve the same mechanism.

The product level distribution for $O(^1D) + H_2 \to OH(v) + H$ has also been discussed in many reports[46] with some remaining disagreement.[47] Studies indicate a broad, fairly constant distribution, with measured values of $\langle f_v \rangle = 0.33$[48] and $\langle f_v \rangle = 0.39$[49] Analogous to the reaction $N(^2P) + O_2 \to NO(v,J) + O$, mentioned above, $O(^1D) + H_2$ generates product states OH(v,J) with large values of J. Molecular symmetry considerations show that the $O(^1D) + H_2$ reaction can occur on two different surfaces to give product species, one surface involving direct hydrogen atom transfer, and one surface a metastable intermediate.[6] The second mechanism, using $O(^1D)$ insertion to form a short-lived H–O–H intermediate which then dissociates, is thought to be the predominant channel.[47]

For $N(^2D) + H_2 \to NH(v) + H$, the observed linear surprisal plot is consistent with a single formation mechanism. Unlike reported product v distributions of the $O(^1D) + H_2$ reaction, the NH(v) product distribution (Table II) disfavors $v = 0$ product. Also, the average NH(v) product energy $\langle f_v \rangle = 0.44$ is similar to that of the HF(v) product of F + HR reactions, discussed above. These observations suggest a direct abstraction mechanism, as opposed to a mechanism that involves an H–N–H intermediate. Clearly, however, further study is needed in order to elucidate the mechanism for the $N(^2D) + H_2$ reaction, including experimental study of NH(v,J) nascent rotational states, which could not be probed in the current work. Finally, this investigation points up the need for an accurate determination of the H–N–H potential surface in order to predict the reaction dynamics.

VIII. SUMMARY

Rate parameters for NH(v) creation and vibrational relaxation by Ar, N_2, and H_2 have been measured. The reac-

tion $N(^2D) + H_2 \rightarrow NH(X,v\leq 3) + H$ forms NH in excited vibrational states. Relaxation rate constants $k_{v=1\text{-}3}$ ($M = N_2, Ar, H_2$) have been measured for the first time. The relaxation rate constants for N_2 and Ar are small, with a v dependence intermediate between linear and quadratic; upper limits were determined for rate constants $k_{v=1\text{-}3}(H_2)$. The effects of beam-created species on $NH(v)$ quenching have been examined through both detailed reaction modeling and observation. Experimental conditions were chosen which minimized such effects.

The nascent $NH(v)$ vibrational state distribution has been measured as the ratio of fitted creation rates for $v = 1$–3, also for the first time. A statistical model using the surprisal formalism has been used to obtain an estimate for the relative yield of $NH(v = 0)$, which is not detected in our experiment. The nascent product distribution is more highly excited than the statistical prediction, with much less product in $v = 0$ than predicted. The surprisal analysis is consistent with the reaction $N(^2D) + H_2$ as the single operative mechanism for $NH(v)$ formation, and suggests that the reaction involves a direct H atom abstraction rather than a long-lived intermediate.

ACKNOWLEDGMENTS

J. A. D. and D. J. F. gratefully acknowledge support provided by the Geophysics Scholarship program, administered by the Southeastern Conference for Electrical Engineering Education under contract with the Air Force Office of Scientific Research (AFOSR). We thank Bill Marinelli of Physical Sciences Inc. for making available to us the results of his $NH(v)$ emission intensity calculations. This work was supported in part by the AFOSR under Task 2310G4.

[1] W. Hack and A. Wilms, J. Phys. Chem. **93**, 3540 (1989).
[2] F. Freitag, F. Rohrer, and F. Stuhl, J. Phys. Chem. **93**, 3170 (1989).
[3] R. K. Hanson and S. Salimian, "Survey of Rate Constants in the N/H/O System," in *Combustion Chemistry*, edited by W. C. Gardiner, Jr. (Springer-Verlag, New York, 1984).
[4] E. M. Goldfield and K. P. Kirby, J. Chem. Phys. **87**, 3986 (1987).
[5] B. D. Green and G. E. Caledonia, J. Chem. Phys. **77**, 3821 (1982).
[6] R. J. Donovan and D. Husain, Chem. Rev. **70**, 489 (1970).
[7] L. G. Piper, M. E. Donahue, and W. T. Rawlins, J. Phys. Chem. **91**, 3883 (1987).
[8] J. A. Dodd, S. J. Lipson, and W. A. M. Blumberg, J. Chem. Phys. **92**, 3387 (1990).
[9] G. E. Caledonia, B. D. Green, and R. E. Murphy, J. Chem. Phys. **71**, 4369 (1979).
[10] M. Forman, J. Opt. Soc. Am. **56**, 908 (1966).
[11] L. Mertz, Infrared Phys. **7**, 17 (1967).
[12] W. J. Marinelli (personal communication).
[13] E. M. Goldfield (personal communication).
[14] J. Tellinghuisen, Comput. Phys. Commun. **6**, 221 (1974).
[15] K. P. Huber and G. Herzberg, *Constants of Diatomic Molecules* (Van Nostrand Reinhold, New York, 1979).
[16] J. Eccles and D. Malik, Quantum Chem. Prog. Exch. Bull. **13**, 407 (1981).
[17] W. J. Marinelli and L. G. Piper, J. Quant. Spectrosc. Radiat. Transfer **34**, 321 (1985).
[18] J. B. Tatum and J. K. G. Watson, Can. J. Phys. **49**, 2693 (1971).
[19] D. Boudjaadar, J. Brion, P. Chollet, G. Guelachvili, and M. Vervloet, J. Molec. Spectrosc. **119**, 352 (1986).
[20] C. Chackerian, Jr., G. Guelachvili, A. Lopez-Pineiro, and R. H. Tipping, J. Chem. Phys. **90**, 641 (1989).
[21] W. H. Press, B. P. Flannery, S. A. Teukolsky, and W. T. Vetterling, *Numerical Recipes* (Cambridge U.P., New York, 1986).
[22] B. D. Green, G. E. Caledonia, R. E. Murphy, and F. X. Robert, J. Chem. Phys. **76**, 2441 (1982).
[23] C. Zetzsch and F. Stuhl, Ber. Bunsen-Ges. Phys. Chem. **85**, 564 (1981).
[24] L. G. Piper, J. Chem. Phys. **70**, 3417 (1979).
[25] S. T. Gibson, J. P. Greene, and J. Berkowitz, J. Chem. Phys. **83**, 4319 (1985).
[26] C. Zetzsch, Habilitationsschrift, Ruhr-Universitat Bochum, 1978.
[27] J. D. Mertens, A. Y. Chang, R. K. Hanson, and C. T. Bowman, Int. J. Chem. Kin. **21**, 1049 (1989).
[28] J. A. Miller and C. T. Bowman, Prog. Energy Comb. Sci. **15**, 287 (1989).
[29] J. E. Spencer and G. P. Glass, Chem. Phys. **15**, 35 (1976).
[30] R. J. Gordon, Comm. At. Mol. Phys. **21**, 123 (1988).
[31] B. D. Green, G. E. Caledonia, W. A. M. Blumberg, and F. H. Cook, J. Chem. Phys. **80**, 773 (1984).
[32] D. Husain, S. K. Mitra, and A. N. Young, J. Chem. Soc., Faraday Trans. 2 **70**, 1721 (1974).
[33] C. -L. Lin and F. Kaufman, J. Chem. Phys. **55**, 3760 (1971).
[34] R. J. Kee, J. A. Miller, and T. H. Jefferson, CHEMKIN: A General-Purpose Problem-Independent, Transportable, FORTRAN Chemical Kinetics Code Package, Report SAND 80-8003, Sandia Laboratories, Albuquerque, NM (1980).
[35] L. R. Pederson, T. Sawada, J. N. Bass, and A. E. S. Green, Comp. Phys. Commun. **5**, 239 (1973).
[36] R. E. Center, Phys. Fluids **13**, 79 (1970).
[37] J. C. Person, "Modeling of the Production of Vibrationally Excited NH in N_2/H_2 Mixtures," in AFGL-TR-88-0186, Geophysics Laboratory, Hanscom AFB, MA (1988).
[38] A. Ben-Shaul, R. D. Levine, and R. B. Bernstein, J. Chem. Phys. **57**, 5427 (1972).
[39] J. C. Polanyi and K. B. Woodall, J. Chem. Phys. **57**, 1574 (1972).
[40] C. E. Moore, *Atomic Energy Levels*, National Bureau of Standards Circular 467 (U. S. Gov. Printing Office, Washington, D.C., 1958).
[41] C. W. Bauschlicher, Jr., and S. R. Langhoff, Chem. Phys. Lett. **135**, 67 (1987).
[42] B. S. Agrawalla and D. W. Setser, J. Phys. Chem. **90**, 2450 (1986).
[43] W. T. Rawlins, M. E. Fraser, and S. M. Miller, J. Phys. Chem. **93**, 1097 (1989).
[44] D. S. Perry and J. C. Polanyi, Chem. Phys. **12**, 419 (1976).
[45] J. C. Polanyi and J. L. Schreiber, Faraday Discuss. Chem. Soc. **62**, 267 (1977).
[46] P. M. Aker and J. J. Sloan, J. Chem. Phys. **85**, 1412 (1986) and references therein.
[47] C. B. Cleveland, G. M. Jursich, M. Trolier, and J. R. Wiesenfeld, J. Chem. Phys. **86**, 3253 (1987).
[48] Y. Huang, Y. Gu, C. Liu, X. Yang, and Y. Tao, Chem. Phys. Lett. **127**, 432 (1986).
[49] J. E. Butler, R. G. MacDonald, D. J. Donaldson, and J. J. Sloan, Chem. Phys. Lett. **95**, 183 (1983).